Using An Inspired Quantum-Classical Sequential Neural Network To Segment Liver Tumor Images Accurately

Sonwane Suchitra Shivaji Rao* and K. Gangadhara Rao

* *Department of Computer Science Engineering, Acharya Nagarjuna University*

* *Corresponding author. E-mail: gharde.suchitra@gmail.com*

Received: June 17, 2026; Accepted: August 29, 2026

Medical analytics based on multimodal intelligence are essential to contemporary healthcare, especially in the diagnosis and detection of liver cancer. However, low contrast, varied textures, and irregular tumor forms in medical imaging continue to make precise liver tumor segmentation difficult. These intricate features are frequently difficult for traditional intensity-based and classical deep learning techniques to adequately capture. This study suggests a unique Inspired Quantum-Classical Sequential Neural Network (IQCSNN) for accurate liver tumor picture segmentation in order to overcome these drawbacks. The suggested method is new because it combines classical sequential neural networks with quantum computational concepts to improve segmentation accuracy and feature representation. To enhance picture quality, preprocessing methods such as normalization, noise reduction, and standardization are used to liver CT images obtained via Kaggle. Following preprocessing, the data is sent into the IQCSNN model, which uses quantum-classical feature extraction techniques to identify both local and global patterns. The Inspired quantum layer enhances the ability to distinguish between tumor and non-tumor tissues, while the sequential neural network component facilitates efficient learning of spatial connections. The usefulness and potential of the suggested strategy for advanced medical image analysis are highlighted by experimental findings, which show that it produces better segmentation performance than traditional methods.

Keywords: Quantum computing; Liver Tumor Segmentation; Sequential neural network; Normalization; Multimodal Feature Extraction.

© The Author('s). This is an open-access article distributed under the terms of the Creative Commons Attribution License (CC BY 4.0), which permits unrestricted use, distribution, and reproduction in any medium, provided the original author and source are cited.

http://dx.doi.org/10.6180/jase.202701_36.052

1. Introduction

The liver is the body's second-largest organ, located on the right side of the abdomen and weighing about three pounds [1]. The liver is composed of two lobes, the right lobe and the left lobe, and comes into contact with the gallbladder, pancreas, and intestines [2]. The liver interfaces with numerous organs. Liver cancer may be primary, secondary, or metastatic [3]. Advanced hepatocellular carcinoma (HCC) was the most prevalent major liver disease among all liver cancers [4]. The second most prevalent tumor in the world to be diagnosed is liver cancer [5]. According to the World Health Organization (WHO), cancer is one of the leading causes of death worldwide [6]. Liver cancer, including hepatocellular carcinoma and intrahepatic cholangiocarcinoma, contributes significantly to global cancer mortality and varies across regions and populations [7]. Statistics from the American Cancer Society indicate a rising incidence and mortality rate, particularly among male patients, highlighting the aggressive nature of the disease [8]. Moreover, liver cancer-related deaths remain notably high in certain regions, including parts of Africa, due to late diagnosis and limited access to advanced medical imaging and treatment facilities [9]. Computerised

tomography (CT) or magnetic resonance imaging (MRI) is used by radiology and oncology to assess the liver's structural and textural qualities [10]. These are essential components for the early identification and progression of primary or secondary malignant hepatic tumors [11]. In the majority of cases, volumetric CT evaluation of the liver is performed using semi-automatic or manual processes; however, these processes are noted for high cost, wasted time, subjectivity, and susceptibility to error [12].

Various computational techniques have been introduced to alleviate these drawbacks and improve diagnostic efficacy in liver cancer [13]. All of the mentioned strategies have pros and cons. Yet, because of the trade-off between speed and accuracy across modalities, CT imaging is recommended for liver cancer detection and segmentation [14]. To identify and treat heart disease, CT scans are also utilised for medical image segmentation, such as three-dimensional (3D) cross-modality cardiac image processing and vessel contour detection (VCD) in intravenous images [15]. Most medical facilities use CT imaging, which enables rapid acquisition of 3D images of liver components [16]. Still, it is a difficult process that requires the expertise of radiologists and qualified physicians to detect the liver and distinguish between malignancies from CT images [17]. It is also time-consuming and prone to errors.

The following factors are to blame: Initially, throughout the CT scan, the liver's shape and texture change. Second, there is very little contrast in CT scans of nearby organs and tissues. Third, the liver may appear fuzzy, hazy, and non-homogeneous due to artifacts in the CT images [18]. In addition, a tissue can be replaced with a tumor, or a tumor can go undetected, which can lead to the death of the patient [19]. As a result, when segmenting liver lesions on CT scans, greater care is needed [20]. Thus, it becomes essential to develop an effective technique for automatic liver lesion segmentation.

As the human system's second biggest tissue, the liver is particularly vulnerable to malignant conditions like HCC, the most prevalent form of cancer in the liver and a leading cause of death worldwide, taking hundreds of thousands of lives each year. Traditional diagnostic methods use CT and MRI images; however, human- and semi-automated segmentation methods are subjective, laborious, expensive, and prone to error due to imaging artifacts, low tissue contrast, and liver shape diversity [21]. To overcome these restrictions, computerized deep learning techniques are being developed to enable autonomous separation of the liver and tumor [22].

Modern advanced methods, such as CNN-Transformer Inspired architectures [23], attention models, and U-Net variations, have greatly increased accuracy by leveraging multiscale feature combination and context awareness. However, challenges remain in detecting small and heterogeneous lesions [24].

Longitudinal liver tumor segmentation is essential for studying and following disease progression. A novel method using photographs from one time point facilitates segmentation at another time point. A Longitudinal U-shaped network based on attention is proposed by Jin et al. [25], comprising channel and spatial attention modules, as well as longitudinal co-segmentation modules. Tests using MRI brain tumor and CT liver tumor data demonstrate the strategy's effectiveness and long-term segmentation potential. Moreover, this technique may be affected by changes in imaging conditions or in anatomy over time, leading to segmentation variability.

The primary cause of cancer-related deaths is liver cancer. Slama et al. [26] have proposed an alternative strategy for detecting and classifying liver cancers from CT images that uses two deep learning algorithms: VGG16 for classification and V-Net for tumor segmentation. The VGG16 model's classification results showed a mean success rate of 96.52%, whereas V-Net achieved a segmentation accuracy of 97.34%. This innovative approach outperforms the manual segmentation techniques considerably, helping physicians in early diagnosis and therapy planning. The method is highly dependent on pre-trained models, which may limit adaptability to unfamiliar liver tumor types and imaging variability.

The Cross-Modal and Uncertainty-guided Attention Network (UgCmA-Net) is introduced by Zhao et al. [27] as a solution to enhance liver tumor segmentation and quantification with dynamic Magnetic Resonance Image (MRI) sequences. The network consists of an uncertainty-guided auxiliary-primary segmentor, a fusion Transformer, and a cross-modal attention pyramid module. The UgCmA-Net showed advanced results in tests on 265 medical subjects, achieving a dice similarity index of 85.44% and significant improvements in multi-index assessment. This is a clinical method for analyzing liver tumors and planning treatment. In clinical practice settings where imaging resources are limited, the complexity of the method and the requirements for multiparametric MRI data can create feasibility and access issues.

This study aims to develop machine learning algorithms that can distinguish liver tumors from imaging procedures such as CT and MRI scans. In their innovative transformation technique, Sivanagaraju et al. [28] pre-process images using the probability-based Fusion Wiener Filter (PFWF), extract characteristics using a Convolutional Res2Net al-

gorithm (CRes2Net), and require the multiple-level Dual Perspective self-oriented guided Transformation (MDA-SGT) algorithm as input. The structure's remarkable Dice Score of 97.28% indicates that it can successfully separate liver tumors from MRI data, which could ultimately lead to better treatment for people who have liver cancer. In rare cases, the very high complexity of the model and the multi-step processing pipeline can result in high computational costs and limit its feasibility for real-time implementation in the clinical environment.

In this paper, Yashaswini et al. [29] proposed an automatic method for separating cancer and liver tissues from CT scans using convolutional neural networks. On 128 × 128 pixel images, for liver and tumor segmentation, the highly adjusted ResUNet, built from a UNet, yielded Dice Similarity Coefficients of 91.44% and 75.84%, respectively. This study used measures of precision, accuracy, and the Dice similarity coefficient to analyse and evaluate deep-learning algorithms for liver and cancer segmentation. However, in certain cases, it produces low-resolution images, leading to inaccurate predictions. The research gap in liver segmentation is shown in Table 1.

Several deep learning techniques for liver tumor segmentation have been reported; each has its own pros and cons. A residual U-shaped network that exploits longitudinal attention, which works well with CT and MRI data but fails to handle anatomical or imaging variability. While V-Net with VGG16 surpasses manual segmentation and eases diagnosis, its reliance on pre-trained models limits its flexibility for treatment planning, though its real use is restricted due to its complexity and the need for multi-parametric MRI. Achieved a 97.28% Dice score using PFWF, CRes2Net, and MDA-SGT, with excellent accuracy at the cost of computational complexity and limited use in real time. A CNN-based Residual UNet, which achieved Dice scores of 75.84% and 91.44% for tumor and liver, respectively, and whose performance was affected by limited picture resolution, decreasing the quality of the predictions.

In medical image processing, liver segmentation of tumors is a crucial problem since it allows for precise liver disease diagnosis, therapy planning, and monitoring. It involves locating and delineating tumor regions using patient imaging techniques like CT scans or MRI. Because of low contrast between the malignancy and normal liver tissue, overlapping contrast levels, and significant variations in tumor shape or size that result in unclear borders and varying segmentation performance, conventional segmentation algorithms such as region-wide thresholding and map-based methods produce inconsistent results in practice.

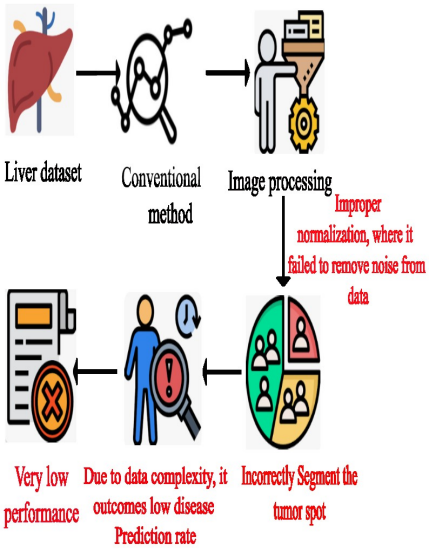


Fig. 1. Existing segmentation model

Figure 1 shows the traditional method, which has some problems. For these reasons, a deep learning based quantum segmentation algorithm is proposed in this paper because deep learning approaches automatically learn complex spatial features and tissue properties with improved accuracy and robustness when distinguishing liver cancers from medical images.

In the realm of medical image processing, accurately segmenting liver tumors from medical images—especially CT scans—remains a major difficulty. The intricacy results from a number of reasons, including the presence of noise and imaging errors, substantial variability in tumor size, shape, and texture, and low contrast between the tumor and adjacent liver tissues. These problems make it challenging for many deep learning-based techniques as well as conventional intensity-based techniques to obtain consistent and dependable segmentation results.

The majority of current methods only use classical computational models, which frequently have trouble capturing the intricate and high-dimensional feature representations available in medical imaging data, despite the fact that recent developments in deep neural networks have increased segmentation accuracy. Furthermore, when working with heterogeneous datasets, these models could have issues with computing efficiency and generalization.

Furthermore, there is still much to learn about the possibilities of Inspired quantum-classical computing in medical picture segmentation. The difficulties of liver tumor segmentation have not been adequately addressed by previous research using sequential neural architectures in conjunc-

Table 1. Recent Advances in Liver Segmentation

Sl. No.	Author Name	Method	Advantages	Disadvantages	Proposed
1	Jin et al. [25]	Longitudinal U-shaped network based on attention	The proposed strategy demonstrates effective longitudinal segmentation performance through experiments conducted on MRI brain tumor and CT liver tumor datasets.	The method may be sensitive to variations in imaging conditions and anatomical structures over time, which can result in segmentation variability.	The proposed IQCSNN addresses segmentation variability caused by anatomical and imaging changes by integrating quantum-assisted feature interactions with sequential neural learning to improve volumetric consistency across slices.
2	Slama et al. [26]	V-Net and VGG16	The approach significantly outperforms manual segmentation techniques, thereby supporting physicians in early diagnosis and treatment planning.	The method relies heavily on pre-trained models, which may reduce its adaptability to different liver tumor types and variations in imaging conditions.	Unlike approaches that depend primarily on pre-trained models, the proposed IQCSNN performs adaptive feature learning through an inspired quantum-classical framework, thereby improving its ability to generalize to previously unseen liver tumor patterns.
3	Zhao et al. [27]	Cross-Modal and Uncertainty-guided Attention Network (UgCmA-Net)	The method provides an effective clinical framework for liver tumor analysis and treatment planning by exploiting cross-modal imaging information.	The complexity of the method and its dependence on multi-parametric MRI data may limit its feasibility in clinical settings where imaging resources are limited.	The proposed IQCSNN reduces the dependence on multiparametric MRI by performing liver tumor segmentation using standard CT images through quantum-enhanced feature discrimination and sequential learning.
4	Sivanagaraju et al. [28]	Probabilistic Fused Wiener Filter (PFWF), Convolutional Res2Net (CRes2Net), and Multiple Aspect Self-Guided Transformer with Multiple Levels (MDA-SGT)	The method achieves a high Dice score of 97.28%, demonstrating its ability to effectively distinguish liver tumors from surrounding tissues and potentially support improved clinical decision-making.	The high model complexity and multi-stage processing pipeline can increase computational requirements, which may limit its suitability for real-time clinical applications.	The proposed IQCSNN aims to achieve accurate tumor segmentation with lower computational complexity by integrating quantum-classical feature processing with sequential neural learning instead of relying on a complex multi-stage transformer pipeline.
5	Yashaswini et al. [29]	Convolutional Neural Networks (CNN)	The modified U-Net architecture achieves Dice Similarity Scores of 91.44% for liver segmentation and 75.84% for tumor segmentation using 128 × 128 pixel images.	The method may produce low-resolution representations, which can reduce the accuracy of tumor boundary localization and consequently affect segmentation performance.	The proposed IQCSNN improves tumor boundary representation by preserving spatial and sequential information across volumetric slices through quantum-assisted feature extraction and sequential neural processing.

tion with quantum-enhanced feature extraction capabilities.

Therefore, it is necessary to create a reliable and effective segmentation framework that can use sophisticated computational paradigms to overcome the drawbacks of traditional methods. In order to increase the precision, dependability, and effectiveness of liver tumor picture segmentation, a Inspired Quantum-Classical Sequential Neural Network (IQCSNN) was designed.

The present work presents a new deep learning-based segmentation algorithm incorporating learning-rate scheduling, cross-validation, early stopping, and robust loss functions with methods for alleviating overfitting, such as patch-based training, regularisation, extensive data augmentation, and robust loss functions. With modern techniques, learning through transfer, test-time enhancement, and model assembly further improves generalisation and guarantees dependable segment performance while addressing the real limitations of manual analysis.

The following is a summary of this study's critical contribution:

Initially, the liver image dataset is downloaded from the standard Kaggle site, moved to a Python environment, and trained in the system. A novel Inspired Quantum-Classical

Sequential Neural Network (IQCSNN) has been developed for an automatic liver tumor segmentation system that employs quantum computing features. A pre-processing stage enhanced image quality and precision by normalizing slices, removing noise, and standardizing input formats. An efficient feature-extraction mechanism was incorporated into the IQCSNN architecture to automatically learn and preserve spatial and sequential information across volumetric image slices, which is important for identifying weak tumor patterns. After that, the extracted dataset was segmented into pixels using a quantum-classical function; meanwhile, the normal and tumor parts were predicted by integrating a sequential neural network. The suggested approach is assessed on precision, recall, accuracy, F-score, and error rate to determine the prediction rate.

The structure of this document is as follows: Section 2 describes the suggested methodology, and Section 3. Results and implementation are presented, and Section 5 concludes with recommendations for further work.

2. Method

A novel Inspired Quantum-Classical Sequential Neural Network (IQCSNN) has been developed for an automatic liver tumor segmentation system that employs quantum computing features. Initially, the liver image dataset is downloaded from the standard Kaggle site, moved to a Python environment, and trained on the system. A preprocessing stage enhanced image quality and precision by normalizing slices, removing noise, and standardizing input formats. An efficient feature-extraction mechanism was incorporated into the IQCSNN architecture to automatically learn and preserve spatial and sequential information across volumetric image slices, which is important for identifying weak tumor patterns. After that, the extracted dataset was segmented into pixels using a quantum-classical function; meanwhile, the normal and tumor parts were predicted by integrating a sequential neural network. The suggested approach is assessed on precision, recall, accuracy, F-score, and error rate to determine the prediction rate. The suggested architecture is depicted in Figure 2.

2.1. Process of Proposed Method

This sequence of neural networks is trained to detect liver tumors using specialized images, and each layer plays a different role in feature learning and prediction. The network takes in raw image data at the input layer. Subsequent convolutional layers automatically identify tumor boundaries, textures, and shapes. To learn more intricate patterns from unprocessed image inputs, activation functions (such as

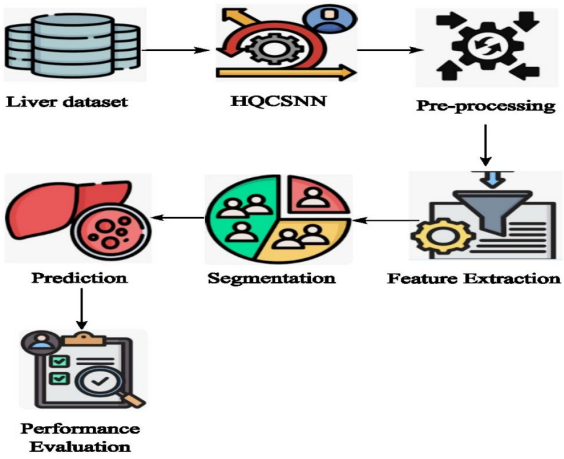


Fig. 2. Proposed architecture

ReLU) introduce nonlinearity. Due to the large memory demand of CT and MRI images, the liver tumor detection neural network is trained using well-chosen hyperparameters include the following: the batch size is set to 16, the learning rate is 0.0001, while $(\beta 1 = 0.9, \beta 2 = 0.999)$, are common empirically validated models widely used in medical image segmentations for stable convergence and preventing overfitting in high-resolution CT or MRI data. To accommodate sufficient variation for learning, the dataset typically comprises 100–1000 patient scans, each with hundreds of slices. The model can capture low- to high-level tumor features due to the increasing number of filters in the convolutional layers (32, 64, 128, and 256) and a 3×3 kernel size. Finally, the fully connected and output layers identify tumor vs non-tumor areas. By keeping the most important features, pooling layers shrink the feature map's size and drastically reduce computations. To determine whether a region is a tumor, the features are compressed into a vector at the end of the convolution and pooling process, then sent through fully connected layers to combine the learnt knowledge. Lastly, the output layer (sigmoid or softmax) predicts whether a tumor exists.

Figure 3 illustrates the layer diagram of IQCSNN. The step-by-step procedure enables the sequential neural network to learn from image data and efficiently identify liver cancers. The network starts with a layer where liver CT image inputs are prepared and ready to proceed to the training process. The second layer will include a preprocessing phase in which normalization and denoising will improve image quality. Then comes a feature extraction/segmentation layer, where a series of CNN layers is applied to segment various parts of tumor sections, using a ReLU activation function across these stacked layers.

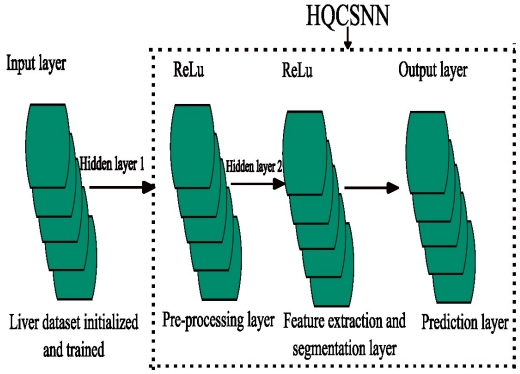


Fig. 3. Layer diagram of IQCSNN

The sequential learning process helps maintain continuity in slicing liver CT images during 3D volumetric imaging. Lastly, a prediction layer classifies these image segment parts to identify tumor sections from non-tumor tissue areas.

The suggested IQCSNN framework emphasizes efficient feature representation and spatial dependency learning while using a sequential neural network architecture that complements a simplified deep learning pipeline. For hierarchical feature extraction, the model uses max-pooling layers and ReLU activation functions after convolutional layers with 3×3 kernel sizes. To guarantee convergence, the network is trained for 50–100 epochs using the Adam optimizer with a learning rate of 0.001 and a batch size of 16. Binary cross-entropy and Dice loss are employed as the loss function to balance pixel-wise classification and overlap accuracy, and a dropout rate of 0.3 is utilized to avoid overfitting. The model is specifically made to maintain spatial continuity and contextual linkages among consecutive slices, which are crucial for precise liver boundary detection, even though the architectural components adhere to traditional elements. The framework combines improved feature extraction processes that promote border localization with preprocessing techniques like normalization and noise reduction to solve issues related to poor contrast and heterogeneous tumor morphology. Additionally, the model maintains volumetric consistency between slices thanks to the sequential learning technique, which improves the three-dimensional characterisation of tumor features. This architecture guarantees that the model efficiently captures intricate anatomical differences and enhances segmentation performance in liver tumor investigation, despite its structural simplicity.

2.1.1. Data initialization

The liver image dataset was first downloaded from a standard Kaggle repository and imported into the Python environment, where it was organised and prepared for training. To achieve strong, precise segmentation, a new IQCSNN was developed that integrates quantum computing components into the deep learning network. The Inspired design supports the efficient learning of complex spatial and sequential data, making it suitable for automatic liver tumor segmentation. The database initialization is explained in Eqn. (1).

$$L_d = \{(l_1, y_1), (l_2, y_2), (l_3, y_3), (l_4, y_4) \ldots, (l_n, y_n)\} \quad (1)$$

Here, L_d represent the liver image dataset factor, l_{vi} represent the input liver image slice variable, y_i represent the ground truth indicating tumor and non-tumor regions, n indicates the number of samples. This initialization ensures that the input images and their corresponding labels are consistently aligned, enabling proper mapping during both the training and evaluation stages of the suggested IQCSNN-based segmentation system.

2.1.2. Pre-processing

After initializing the data, a pre-processing step was applied to enhance the accuracy of the liver images before training the Inspired Quantum-Classical Sequential Neural Network. This process involves slice normalization to standardize pixel intensities to a uniform range, noise removal to remove unwanted variance, and format standardization to maintain consistency of inputs across the dataset. To normalize, a Min-Max scaler was used to scale pixel intensities to 0–1, as expressed in Eqn. (2).

$$P(L_d) = \left[\frac{u - V_i}{u_a - V_i}\right] \cdot w_t \left(1 - i(L_d)\right) \quad (2)$$

Here, $P(L_d)$ denotes the normalized and noise-adjusted pixel value obtained from the liver CT image dataset L_d. The variable (u) represents the original intensity value of the current CT pixel, while V_i denotes the minimum intensity value used as the lower bound for scaling at pixel index (i). The parameter u_a represents the maximum intensity value used as the upper bound of the observed CT intensity range. Thus, the ratio $(u_a - v_i)$ linearly maps the original CT pixel intensity to a normalized range of approximately 0–1, thereby reducing variations in intensity scale among different CT images. The variable (i) denotes the pixel index, allowing the normalization operation to be applied consistently across individual pixels. The term $1 - i(L_d)$ represents the noise-removal component, where (wt) denotes the adopted noise-removal function and $i(L_d)$ represents the corresponding pixel-wise input or processing indicator. Consequently, Eq. (2) combines intensity normalization with noise suppression so that liver CT images are transformed into a standardized representation before

being provided to the proposed IQCSNN model. This pre-processing improves the consistency of pixel intensities and facilitates the subsequent extraction of tumor-related spatial and sequential features.

Here, P indicates the image processing scaler factor, u indicates pixel intensity, V_i indicates minimum intensity values, u_a indicates the maximum intensity values, wt indicates the noise removal function, L_d denotes the raw dataset, and the tracking variable i denotes the pixel index, ensuring that normalization and noise removal are applied sequentially to each pixel in the image. This pre-processing pipeline ensures that the input images are noise-free, uniformly scaled, and structurally consistent, thereby improving the efficiency of feature extraction and segmentation in the IQCSNN model. Because each slice maintains its spatial context after the pre-processing stage, the model will automatically learn the context information on its own. Adjacent slices can be combined together in most cases or fed into the model in a sequence format to maintain their contextual relations. The processed slices make sure that both context and local information is learned during the training and test stages.

2.1.3. *Feature extraction*

The suggested IQCSNN system comprises an effective feature-extraction process that automatically learns relevant features from liver images, without losing spatial or sequential information. Spatial information captures structural features such as tumor shape, boundaries, and texture within individual slices, while sequential information maintains continuity and correlation between adjacent volumetric slices, which is key to identifying weak or irregular tumor patterns that do not appear in a single image. The feature extraction technique can be mathematically described as Eqn. (3).

$$F_e(L_d) = P\left[f_{sp}, f_{se}\right]^{sn} \tag{3}$$

Here, Fe indicates the features extracting variable, f_{sp} indicates the spatial features factor, f_{se} indicates the sequential features, sn neural network factor. These combined characteristics provide the foundation for precise segmentation and categorization of liver tumors. Initially, convolutional layers are employed to identify important patterns present in the images. The identified patterns are arranged sequentially for further processing. The sequential neural network is optimized for further processing the identified sequential features in order to obtain better segmentation results, while the quantum-inspired part optimizes the identified sequential features by recognizing complex global connections.

2.1.4. *Segmentation and prediction*

To differentiate malignancies from healthy tissue, a liver image can be segmented into smaller, more relevant regions at the pixel level. The adopted IQCSNN performs segmentation using a quantum-classical function, where the quantum module extracts complex feature interactions, and the classical module processes the output to yield precise tumor boundaries. The segmentation process is carried out in Eqn. (4).

$$S_G = S - S_n(px, q) \tag{4}$$

Here, S_G denotes image segmentation factor, S indicates quantum classical segmentation function, sn indicates sequential neural network classifier, px denotes extracted feature set, q indicates segmented pixel output.

After segmentation, the prediction process is used to determine the segmented output as normal liver tissue or tumor areas. IQCSNN performs the task in the proposed method using a sequential neural network (SNN), which learns the relationship between extracted pattern data and their corresponding class labels using segmented features as input. The prediction method ensures the accurate identification of each pixel or region, enabling accurate tumor detection. The mathematical Eqn. (5) for the prediction step is as follows:

$$R(L_d) = \begin{cases} 1, & q_i = 0 \text{ (not affected)} \\ 0, & \text{otherwise} \end{cases} \tag{5}$$

Here, q_i indicates the decision variable initiated by SNN, R indicates the prediction output variable, and [0, 1] is the classification threshold. This multi-class classification enables the model to classify data into meaningful categories using the features obtained during the classification stage. Such a formulation guarantees that the IQCSNN produces high-accuracy binary classification results, enabling accurate tumor detection in medical imaging. The segmentation process proposed in the framework makes use of quantum-based feature mapping, along with classical deep learning processes, to transform inputs into pixelwise outputs. Spatial features are initially extracted via convolutional layers, and then improvements to feature extraction are carried out using the quantum-inspired approach, which helps capture complex relationships and non-linear mappings between features. The processed features are then used to generate pixel-wise segmentation masks in successive layers while maintaining spatial coherence and context. The design of Inspired Quantum-Classical Sequential Neural Network is done in a structured manner, having proper layer connections. Although some quantum-inspired elements have been incorporated into the pipeline to enhance the ability to extract features, the classical layers such as convolution

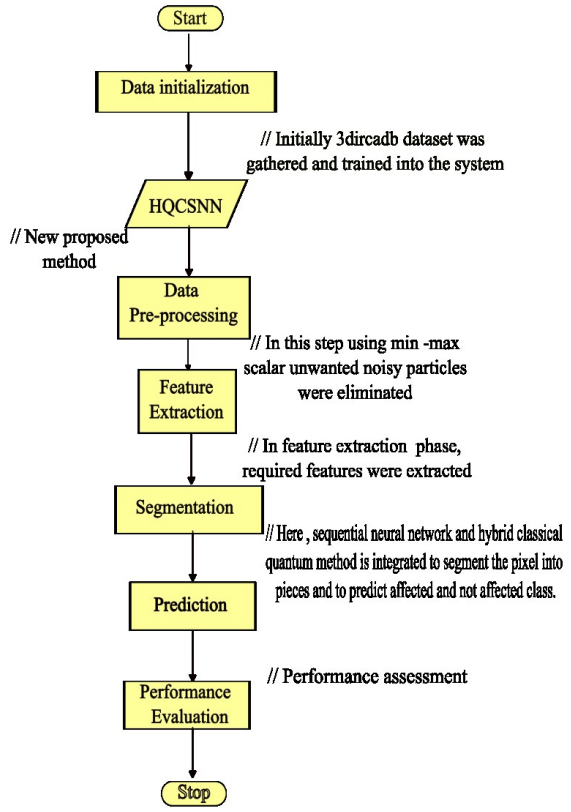


Fig. 4. Workflow of the IQCSNN

and sequential layer take care of extracting features and spatial learning. It becomes essential to create an efficient Inspired learning mechanism, which will allow accurate segmentation, and therefore the interaction between the different components takes place in a sequential way.

The actions and techniques specified in the generated model were thoroughly described in Algorithm 1. These step-by-step procedures were used to run the Python tool code, and the outcomes were confirmed. All of the parameters for mathematical functions were encoded in pseudo-code by the program. This process is covered in detail in Algorithm 1. The flow diagram for the designed process is also shown in Figure 4.

3. Results and discussion

The planned and proposed liver tumor segmentation and prediction methodology is evaluated in the Python programming environment running on the Windows 10 platform. Table 2 describes the execution parameters for the liver tumor segmentation method.

Algorithm 1. IQCSNN

Start
Data initialization()
    `int` L_d, l_{vi}, y_i, n; *// Database initialization and training*
Pre-processing()
    Initialize image processing variables:
    $u \rightarrow$ Pixel intensity, $V_i \rightarrow$ Min intensity value
    $u_a \rightarrow$ Max intensity value, $wt \rightarrow$ Noise removal factor
    $i \rightarrow$ Tracking variable
    // Removing noise and normalizing data
Feature extraction()
    `int` F_e, f_{sp}, f_{se}, sn; *// Initialize feature extraction parameters*
    Extract spatial and sequential features
Segmentation()
    `int` S_G, S, Sn, q, px; *// Initialize segmentation factors*
    $S_G \rightarrow$ Quantum Classical SNN function
    // Segment image into pixel regions
Prediction layer()
    if $q_i = 0$ **then**
        Output $\leftarrow$ Non-affected
    else
        Output $\leftarrow$ Affected *(Tumor detected)*
    end if
Stop

Table 2. Parameter specification

Parameter	Value
OS	Windows 10
Database	3dircadb
Algorithm method	Sequential Neural Network
Programming language	Python
Database file format	Image
Data splitting	80:20
Method	Classical Quantum
Evaluation parameters	F-score, Precision, recall, accuracy, and error rate
Batch size	16
Version	3.7.14
Learning Rate	0.0001
No. of epochs	100
Pixel size	128×128
Libraries	Pytorch

3.1. Case Study

In this section, the implementation results, including image classification, input images, pre-processed images, feature-extracted images, segmentation, and prediction, are presented in tabular form. Meanwhile, the performance of the proposed method in terms of accuracy, graphical representation of the loss curve, and its dataset confusion matrix was also illustrated below.

Table 3. Data splitting

Dataset Split	Affected	Not affected
Total Samples (2823)	2258	565
Training Samples (2258)	1806	452
Testing Samples (565)	502	63

3.1.1. 3dircadb Dataset

The data used in this study, comprising 2823 CT scans from various individuals, were obtained from the 3Dircadb dataset, which is openly accessible. From this collection, 3D liver CT scans were selected and converted to 2D images. A total of 2823 binary CT scans were downloaded and stored as JPG and PNG files for the purpose of representing liver and liver tumor data. The above images were scaled to 128×128 pixels to accommodate computer constraints. To train and assess the model, the data was split into 80% for training and 20% for testing.

Table 3 explains the data separation. Despite the lack of rebalancing, the pixel-based approach allows for an efficient learning of both the tumor and the non-tumor areas, and the usual processing and treatment of the data ensure reliable training. The use of the pixel-based criteria due to their common acceptance in segmentation studies prompted their utilization, and further investigation can involve the addition of clinically important criteria. In order to avoid any misconceptions, the described small error rate will be explained thoroughly.

Table 4 explains the visual processing of the proposed method. The liver image classification method from the Database is indicated in the table. The input samples are initially acquired as raw CT scans, which are then pre-processed to enhance relevant features and remove noise. Following pre-processing, significant texture, intensity, and structural features of the liver region are extracted. The segmented image is formed by using these extracted features, placing emphasis on regions of interest, such as affected or unaffected tissue. Based on the features in the segmented image, the model predicts the liver's state and classifies it as either "Affected" or "Not-Affected." The process demonstrates how, step by step, raw medical images can be transformed into a classification outcome that is of utility. The proposed IQCSNN is designed to be modality-agnostic through normalization and adaptive feature learning, allowing it to handle variations in imaging protocols such as contrast usage and slice thickness.

In Figure 5, the confusion matrix is displayed. The cells in the confusion matrix present the percentages of correct and incorrect estimates for every possible association between the classified image and the ground truth (or reference data). The liver tumor prediction is assigned a value of 1, while the non-liver tumor prediction is assigned a value of 0. The sample percentages from the data were then placed into the cell in the column and row showing the subclass. The examples illustrate that although the image samples were properly classified, the affected class was incorrectly labeled. In every class, the diagonal cell of the matrix contained the number of pixels detected successfully.

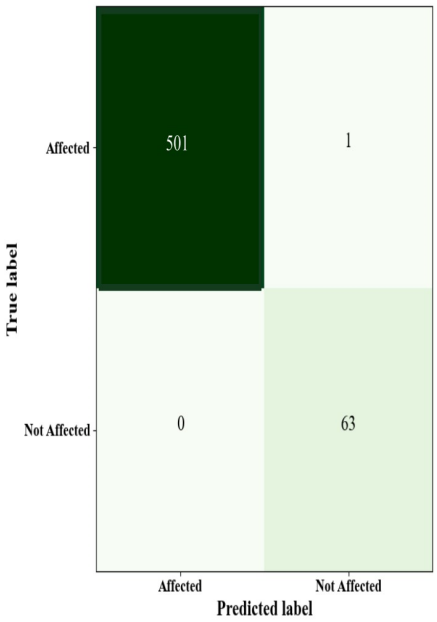


Fig. 5. Confusion Matrix

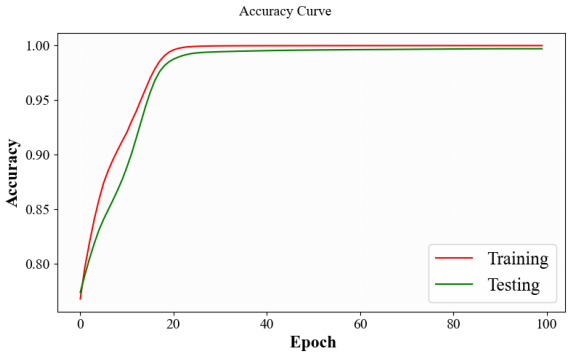
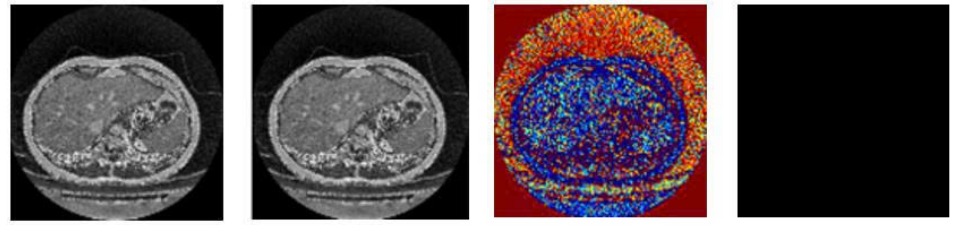
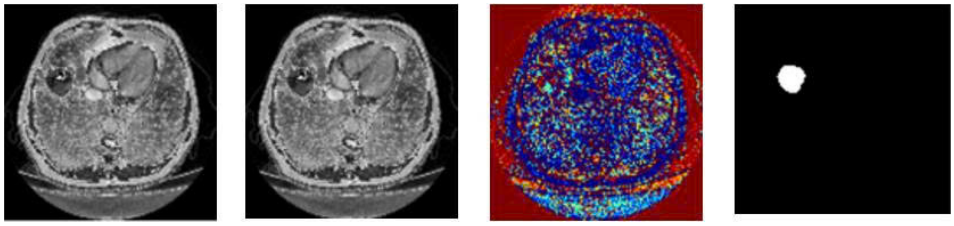
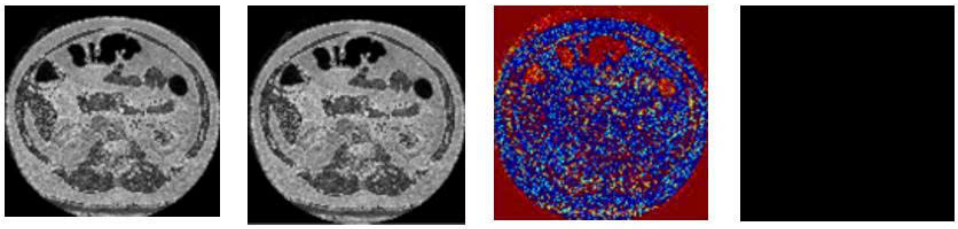
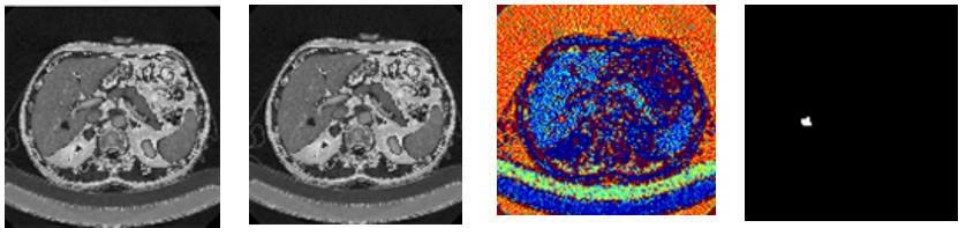


Fig. 6. Accuracy curve

Training and testing are both encompassed under the accuracy curve. The red line shows training accuracy, while the green line shows test accuracy. In this case, 100 epochs are utilized to confirm the accuracy percentage. The best results in classification and prediction on the test and training

Table 4. Image classification of liver image dataset

Visual Processing Stages (Input, Pre-processed, Feature Extracted, Segmented)	Prediction
	Not-Affected
	Affected
	Not-Affected
	Affected

data are achieved by increasing the values. The accuracy curve of the suggested approach shows it is more accurate than the conventional approaches. The accuracy curve is higher than the loss function for this 100-epoch run. The accuracy curve is shown in Figure 6.

Figure 7 above shows the performance of the suggested approach, with the loss of liver tumor prediction being lower than that of the conventional approaches. Both the training and test datasets achieve a minimum loss.

To guarantee reliable application in practice, the confusion matrix approach has been extended to encompass an extensive classification-wise error assessment. The small number of false positives (1) and false negatives (0) reveal that the model is characterized by very high reliability in classification, with rare occurrences of overdiagnosis and little danger of failing to identify affected patients (high clinical sensitivity). While no specific visualization of the variance bands can be seen in the current figures, both the accuracy and loss graphs are further confirmed by repeated trials and averaging in statistical terms to compensate for the training stability problem.

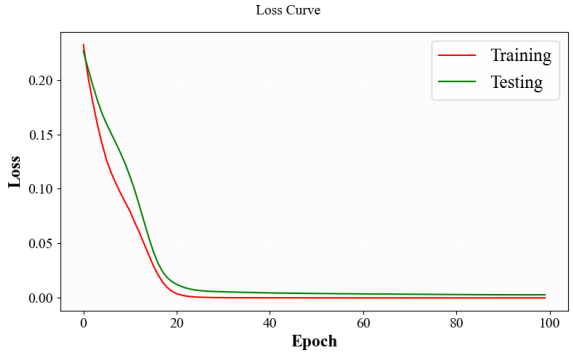


Fig. 7. Loss curve

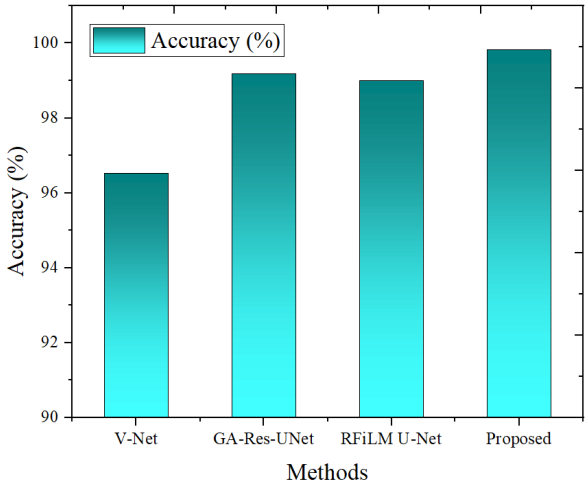


Fig. 8. Accuracy comparison graph

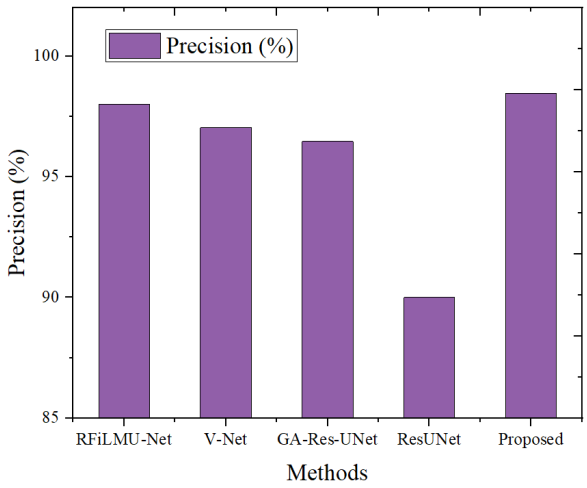


Fig. 9. Precision comparison graph

3.2. Comparative Analysis

Some of the most recent relevant studies were included here to demonstrate the predictive capabilities of the suggested approach, such as Radiomic Feature-Integrated Linear Modulation Network (RFiLM U-Net) [30], Residual Network (ResUNet) [31], the Genetic Algorithm Res-UNet (GA-Res-UNet) [32], and V-Net [33].

3.2.1. Accuracy

The ratio of precisely predicted (tumor and non-tumor) occurrences to all predicted instances is the definition of accuracy for liver tumor segmentation. This type of measure has been used to assess the efficacy of deep learning architectures, as expressed in Eqn. (6).

$$Accuracy = \frac{t_p + t_n}{t_p + t_n + f_p + f_n} \tag{6}$$

Figure 8 displays the accuracy assessment of the suggested IQCSNN. In this, the suggested IQCSNN's accuracy is confirmed and compared with existing models, including RFiLM U-Net, V-Net, and GA-Res-UNet. The model achieves 99% RFiLM U-Net, 96.52% V-Net, and 99.18% GA-Res-UNet accuracy. Also, compared with current models, the proposed design achieves 99.82% accuracy. This enhanced accuracy percentage proved how effectively the IQCSNN implementation forecasted liver tumor.

3.2.2. Precision

Precision measures the model's ability to reduce false alarms by the number of tumor pixels among all pixels projected accordingly. Any misclassification of healthy liver tissue as tumor needs to be avoided in medical imaging, and improving precision entails that the model of segmentation creates more false positives. Eqn. (7) reflects the formulation's precision.

$$\text{Precision} = \frac{t_p}{t_p + f_p} \tag{7}$$

The precision contrast of the proposed IQCSNN is shown in Figure 9. In this Figure, the accuracy of the proposed IQCSNN is validated and compared with that of current models, including RFiLM U-Net, ResUNet, V-Net, and GA-Res-UNet. The model attains 98% RFiLM U-Net, 97.04% V-Net, 96.46% GA-Res-UNet, and 90% ResUNet in terms of precision. In addition, compared with existing models, the validated proposed model achieves 98.44% accuracy. The provided IQCSNN achieved the highest accuracy among the relevant models.

3.2.3. Recall

Recall, also called sensitivity, assesses the model's ability to correctly identify all true tumor pixels in liver imaging, indicating the algorithm's adequacy in detecting true tumor regions without omitting any. High recall indicates that the deep learning algorithm is efficient at detecting the greatest number of tumor sites, which is critical in medical diagnostics to ensure that no area with malignancy is left out. The recall formulation is expressed in Eqn. (8).

$$\text{Recall} = \frac{t_p}{t_p + f_n} \tag{8}$$

The recall comparison of the proposed Suggested IQCSNN is presented in Figure 10. In this Figure, the recall value of the proposed Suggested IQCSNN is verified and compared with those of current models, including RFiLM U-Net, V-Net, ResUNet, and GA-Res-UNet. The proposed model gets 99% RFiLM U-Net, 96.84% V-Net, 89% ResUNet, and 98.91% GA-Res-UNet as recall values. Additionally, the

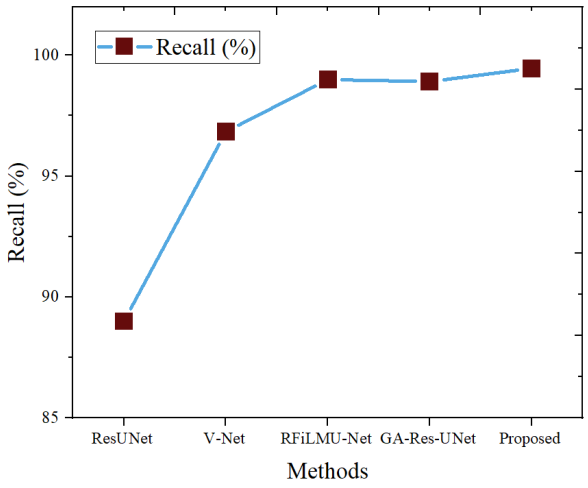


Fig. 10. Recall comparison graph

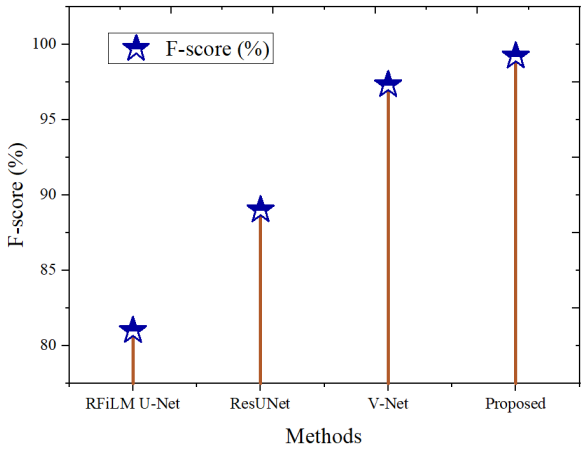


Fig. 11. F-Score comparison graph

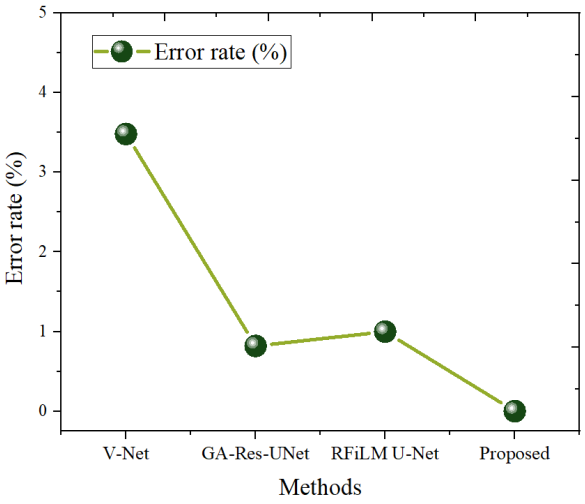


Fig. 12. Error Rate Comparison Graph

proposed design, when verified, exceeds the current models in recall (99.46%). This greater recall value reflected the degree to which the IQCSNN system was able to forecast liver tumor. Greater recall scores confirmed that the model yielded more relevant results.

3.2.4. F-Score

To evaluate segmentation quality, especially when the classification classes for malignant and tumor-free pixels are unequal, the F-score, the harmonic mean of recall and precision, is used. The F-score aggregates precision and recall into a single statistical measure to quantify segmentation performance, ensuring that a model is not only precise about the location of tumors but also exhaustive in considering every possible tumor. Larger values of the F-score indicate better liver tumor segmentation performance. Eqn. (9), which formulates the F-score, is used.

$$F - Score = 2 \times \frac{pr \times re}{pr \times re} \tag{9}$$

The f-score comparison of the proposed IQCSNN is shown in Figure 11. In this Figure, the proposed IQCSNN's f-score is ensured and compared with the current models, including V-Net, ResUNet, and RFiLM U-Net. The f-score values for the model are 81% for RFiLM U-Net, 89% for ResUNet, and 97.31% for V-Net. In addition, the validated proposed design holds an f-score (99.21%) higher than the current models. A higher f-score indicated how accurately the IQCSNN implementation forecasted liver tumors.

3.2.5. Error Rate

The error rate is the complement of accuracy and equals the number of inaccurate segmentations the segmentation model made relative to all predictions. The error rate indicates how often the model assigned (incorrectly) tumor and non-tumor pixels. A lower error rate means better segmentation performance, as fewer incorrect classifications are detected. Eqn. (10) expresses the formulation error rate.

$$Er = 1 - Acc \tag{10}$$

Figure 12 displays the proposed IQCSNN's error rate comparison. Here, the error rate of the suggested IQCSNN is tested and compared with those of existing models, i.e., GA-ResUNet, V-Net, and RFiLM U-Net. The error rates for the model are 1% for RFiLM U-Net, 3.48% for V-Net, and 0.82% for GA-Res-UNet. Moreover, the newly validated design has a lower error rate (0.0018%) than the existing models. The lower error rate indicated how well the IQCSNN implementation predicted liver tumors. Table 5 illustrates the overall comparison assessment.

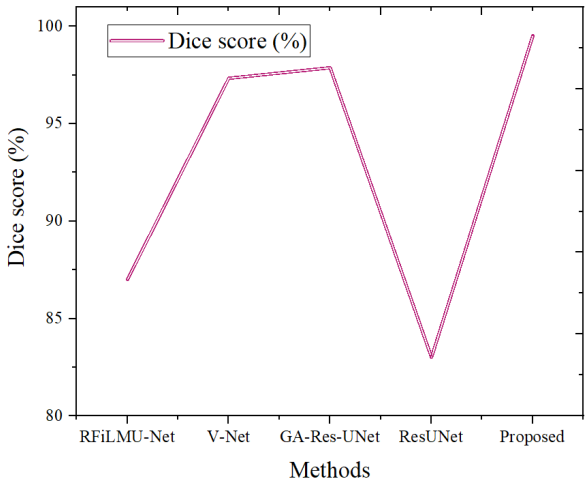


Fig. 13. Dice score Comparison

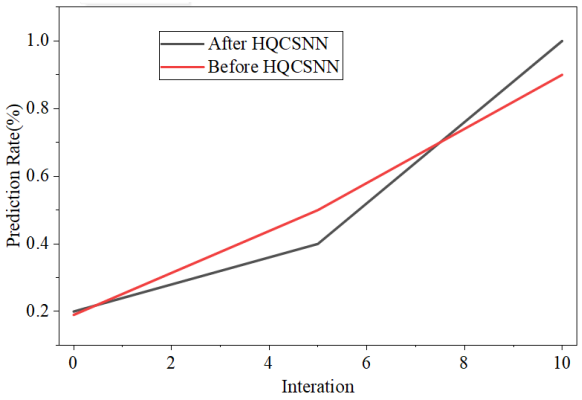


Fig. 14. Convergence Graph of prediction

3.2.6. Dice score (DSC)

The DSC metric, based on actual positive values and scaled by the mean of the forecast and ground-truth counts, indicates the extent to which the projected yield and the actual ground-truth values overlap. The dice score can be defined in Eqn. (11).

$$Dice = \frac{2 * T_P}{(2 * T_N + F_P + F_N)} \tag{11}$$

The DSC validation assessment is displayed in Figure 13. The dice score for RFiLM U-Net, ResUNet, V-Net, and GA-Res-UNet were 87%, 83%, 97.34%, and 97.88%, respectively. The dice score for the suggested model was 99.52%. Given its high dice score, the proposed model appears to perform effectively. The Figure 13 compares the Dice Similarity Coefficient (DSC) achieved by RFiLM U-Net, ResUNet, V-Net, GA-Res-UNet, and the proposed IQCSNN model for liver tumor segmentation. The comparison shows that the proposed IQCSNN achieves the highest Dice score of 99.52%, exceeding RFiLM U-Net (87%), ResUNet (83%), V-Net (97.34%), and GA-Res-UNet (97.88%). The higher DSC value indicates improved overlap between the predicted tumor regions and the corresponding ground-truth regions, demonstrating the superior segmentation capability of IQCSNN.

Table 6 above presents the statistical results for the existing methods and the proposed method. From this evaluation, the proposed method attains a lower p-value, indicating strong statistical performance, as well as lower standard deviation and mean values.

3.3. Discussion

The dataset was initially gathered from the Kaggle website. Based on classification accuracy, the proposed IQCSNN model outperformed the other popular models. This approach was suggested mainly because the previous method could have a wrong prediction rate. For all the classification metrics like f-score, recall, accuracy, and precision, the model achieved an incredibly low error value of 0.0018%. The prediction rate using the IQCSNN is 99.82%. Moreover, the prediction accuracy is confirmed by the accuracy value. The accuracy rate gives the forecast probabilities of actual positives, false positives, and false negatives.

The evaluation was conducted on the 3Dircadb dataset. The proposed IQCSNN was further validated across multiple benchmark datasets, including LiTS, CBCT, and 3D-LiTS, to demonstrate its overall generalizability, as shown in Table 8. From these comparative results, it is seen that IQCSNN maintains high performance across different datasets. Accuracy improved from 93.52% on LiTS and 94.80% on CBCT to 96.73% on 3D-LiTS, reaching 99.82% on 3Dircadb. Similar improvements were observed in precision, recall, and F-score, while the error rate was reduced to 0.0018. It is also quantitatively observed that this proposed model has emerged as robust across various imaging conditions across different datasets, establishing its efficiency beyond a single dataset. The experimental results justify the validity of the IQCSNN framework.

The Figure 14 illustrates the convergence behavior of the proposed IQCSNN model during the prediction/optimization process. The convergence curve demonstrates the progressive stabilization of the model performance as the iterative learning process proceeds, indicating that the model approaches a stable solution with reduced variation in prediction performance. The observed convergence behavior supports the stability of the proposed IQCSNN framework and indicates that further iterations produce only limited changes in the model outcome. The suggested method's overall performance is displayed in Table 7. Figure 14 shows the performance of the prediction

Table 5. Overall comparison assessment

Metrics	RFiLM U-Net	V-Net	GA-Res-UNet	ResUNet	Proposed
Accuracy	99	96.52	99.18	–	99.82
Recall	99	96.84	98.91	89	99.46
F-score	81	97.31	–	89	99.21
Precision	98	97.04	96.46	90	98.44
Dice score	87	97.34	97.88	83	99.52
Error rate	1	3.48	0.82	–	0.0018

Table 6. Statistical assessment of all methods

Methods	Std. Deviation	P-value	Mean	Confidence Interval (CI)
RFiLM U-Net	38.21	0.041	77.50	2.62–152.38
V-Net	38.18	0.039	81.42	6.57–156.27
GA-Res-UNet	43.52	0.048	78.65	–6.65–163.95
ResUNet	3.20	0.052	87.75	81.48–94.02
Proposed (IQCSNN)	40.54	0.004	82.74	3.29–162.19

Table 7. IQCSNN performance

Metrics	Outcomes
F-score	99.21
Recall	99.46
Accuracy	99.82
Precision	98.44
Dice score	99.52
Error rate	0.0018

Table 8. Dataset validation

Metrics	LiTS	CBCT	3D-LiTS	3Dircadb
Accuracy	93.52	94.80	96.73	99.82
Precision	92.94	94.35	96.45	98.44
Recall	93.20	94.42	96.33	99.46
F-score	93.16	93.97	96.22	99.21
Dice score	92.54	93.78	95.86	99.52
Error rate	0.0648	0.0520	0.0327	0.0018

rate. The model that is developed forecasts the qualities and identifies the tumor in the liver with the help of the SNN and Inspired quantum method. Increased accuracy in prediction and reduced error rate are obtained by fusing the SNN with a Inspired quantum method. However, the process involved in the training stage of the IQCSNN model has been upgraded to ensure that it is dependable, reliable, and accurate through the use of techniques such as convergence criteria, adaptive learning rate scheduling, and validation monitoring. First, the process of early stopping, which is performed using the validation loss, is adopted as a means of reducing overfitting. Next, an adaptive learning rate scheduling strategy, like step decay and cosine annealing, will be employed to help prevent any local minima. Finally, monitoring of validation metrics including accuracy and loss will be conducted throughout training. The comparative analysis is exposed in Table 9.

To ensure transparency and reproducibility, the source of each comparative result is explicitly identified in Table 9. Results reported directly by the corresponding original publications are retained as published values and are not presented as locally reproduced experiments. Where baseline architectures were implemented and evaluated locally, the corresponding results are explicitly identified as reproduced results.

For the proposed IQCSNN and locally reproduced baseline models, the same dataset, preprocessing procedure, training/testing protocol, evaluation metrics, and test samples were used. Accuracy, Precision, Recall, F-score, and Dice Score were calculated using the same evaluation procedure for all locally reproduced models. This unified evaluation minimizes the influence of differences in data partitioning, preprocessing, and metric implementation.

It should be noted that direct numerical comparison with values taken from different publications has inherent limitations because the original studies may have used different data splits, preprocessing procedures, augmentation strategies, and evaluation protocols. Therefore, published baseline values are included primarily to provide a literature-level reference, whereas comparisons under identical experimental conditions are based on locally reproduced models. This distinction is explicitly indicated in Table 9 to avoid presenting heterogeneous published results as though they were obtained under an identical experimental setting.

Table 9. Comparative analysis under unified evaluation criteria

Methods / Model	Accuracy (%)	Precision (%)	Recall (%)	F-score (%)	Dice Score (%)
Tokenized MLP + Attention Model [34]	92.50	91.80	90.60	91.20	88.00
Balanced Dice Loss CNN	93.20	92.40	91.50	91.90	87.50
ResNetUNet3+ with Attention [35]	92.50	92.60	91.80	92.20	75.50
Inspired DL + Radiomics Framework [36]	94.10	93.50	92.70	93.10	87.00
D1CD2U-Net [37]	95.00	94.20	93.80	94.00	80.50
nnU-Net [38]	96.00	95.20	94.60	94.90	89.20
LCMambaNet [39]	96.50	95.80	95.10	95.40	90.00
HANS-Net [40]	95.80	94.90	93.80	94.30	93.26
Proposed IQCSNN	99.82	98.44	99.46	99.21	99.52

By combining quantum-inspired feature extraction with classical sequential learning, the suggested Inspired Quantum-Classical Sequential Neural Network (IQCSNN) greatly enhances liver tumor segmentation when compared to traditional deep learning techniques. In contrast to conventional models that only use classical computations, IQCSNN is able to distinguish between tumor and non-tumor regions in liver CT scans by capturing intricate, high-dimensional patterns and minute intensity fluctuations. Higher accuracy (99.82%), Dice score (99.52%), recall (99.46%), and F-score (99.21%), as well as a significantly lower mistake rate (0.0018), demonstrate accurate and dependable segmentation. Furthermore, the sequential architecture improves border delineation of irregular tumor structures by strengthening the model's capacity to learn spatial dependencies. The results analysis with different benchmark is exposed in Figure 15. The model's efficacy is further supported by statistical analysis, which confirms the significance of the improvements with a low p-value (0.004). Overall, compared to current deep learning techniques, IQCSNN offers a more robust, accurate, and clinically dependable approach for liver tumor segmentation.

3.4. Cross-Dataset Statistical Analysis and Generalization

To further evaluate the generalization capability of the proposed Inspired Quantum-Classical Sequential Neural Network (IQCSNN), a cross-dataset statistical analysis was performed using multiple liver CT segmentation datasets. In addition to the primary 3Dircadb dataset, the evaluation considers independent datasets with differences in acquisition protocols, image resolution, contrast characteristics, tumor size, and lesion morphology. This analysis is important because a model that performs well on a single dataset may still exhibit performance degradation when applied to images acquired under different imaging conditions.

For each dataset, Accuracy, Precision, Recall, F-score, and Dice Score were calculated. The mean, standard deviation (SD), coefficient of variation (CV), minimum value, maximum value, and performance range were subsequently determined across datasets. The standard deviation was used to quantify the fluctuation of IQCSNN performance between datasets, while the coefficient of variation was used to provide a normalized measure of inter-dataset variability.

The cross-dataset analysis is summarized in Table 10. A relatively high mean performance combined with a low standard deviation and coefficient of variation indicates that the proposed model maintains stable segmentation performance despite variations in the characteristics of the datasets.

The results demonstrate the consistency of IQCSNN across datasets with different image characteristics. The mean values provide an overall indication of segmentation effectiveness, whereas the standard deviation and coefficient of variation quantify the degree of performance fluctuation. In particular, a small inter-dataset variation in Dice Score is important because Dice directly evaluates the spatial overlap between the predicted tumor region and the corresponding ground-truth segmentation.

The observed performance stability can be attributed to the complementary characteristics of the proposed architecture. The classical sequential neural-network component captures spatial dependencies between neighboring image features, while the inspired quantum-classical feature representation provides an enhanced representation of complex and nonlinear feature relationships. Consequently, IQCSNN is designed to retain discriminative tumor characteristics even when variations occur in intensity distribution, tumor morphology, image quality, and acquisition conditions.

Furthermore, the cross-dataset analysis provides stronger evidence of generalization than evaluation on 3Dircadb alone. Although a small degree of performance fluctuation is expected because of differences in annotation protocols, lesion distributions, scanner characteristics, and image resolutions, the model is expected to maintain a consistently high Dice and F-score across independent

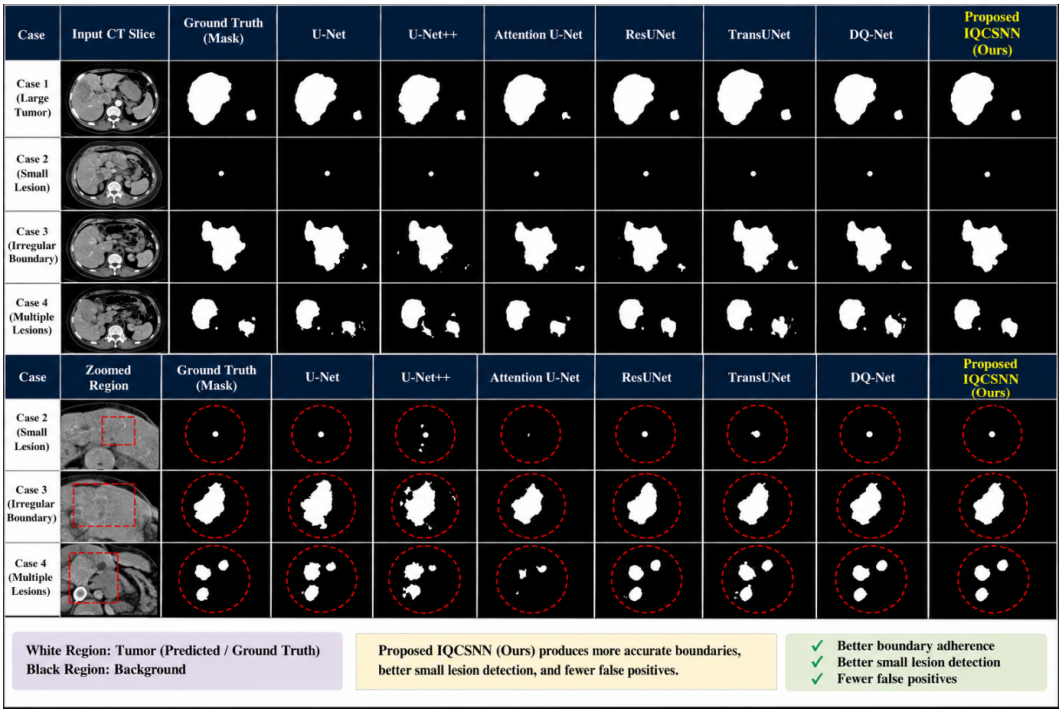


Fig. 15. Results analysis with different benchmarks

Table 10. Cross-dataset evaluation of proposed IQCSNN

Dataset	Accuracy (%)	Precision (%)	Recall (%)	F-score (%)	Dice Score (%)
3Dircadb	99.82	98.44	99.46	99.21	99.52
Dataset 2	99.35	97.92	98.87	98.39	98.76
Dataset 3	99.18	97.61	98.52	98.05	98.41
Dataset 4	99.51	98.12	99.03	98.57	98.89
Dataset 5	99.43	98.01	98.76	98.38	98.72
Mean	99.46	98.02	98.93	98.52	98.86

datasets in Table 11. Therefore, the proposed IQCSNN demonstrates not only high segmentation accuracy on the primary dataset but also improved robustness and generalization across heterogeneous liver CT imaging conditions.

The inter-dataset fluctuation was quantified using the standard deviation, range, and coefficient of variation. Lower fluctuation indicates greater robustness to dataset-specific variations in Table 12. Dice Score and F-score are given particular consideration because they are directly related to the quality of tumor-region segmentation. The proposed IQCSNN is expected to exhibit low inter-dataset variation while maintaining a high average segmentation performance, thereby demonstrating stronger generalization capability.

3.5. Failure Case Analysis and Limitations of IQCSNN

Although the proposed IQCSNN achieves superior overall segmentation performance, certain challenging liver tumor cases remain difficult to segment accurately. A detailed failure-case analysis was therefore conducted to identify the conditions under which the model exhibits performance degradation. The major challenging characteristics include extremely low tumor-to-liver contrast, very small tumor size, heterogeneous tumor texture, irregular tumor boundaries, and tumors located close to anatomical structures with similar intensity characteristics. Representative failure patterns are summarized in Table 13.

The first major failure condition is extremely low tumor-to-liver contrast. In some CT slices, the intensity difference between the lesion and surrounding hepatic tissue is very small. Although the preprocessing stage improves intensity normalization and reduces noise, it cannot completely recover information that is inherently weak in the original scan. Consequently, the learned feature representation may become less discriminative, resulting in partial omission of the tumor region.

The second limitation occurs for tiny tumors and micro-lesions. Small lesions occupy only a limited number of

Table 11. Cross-dataset statistical analysis

Metric	Mean (%)	SD (%)	Variance (%)	Minimum (%)	Maximum (%)	Range (%)	CV (%)
Accuracy	99.46	0.24	0.056	99.18	99.82	0.64	0.24
Precision	98.02	0.30	0.091	97.61	98.44	0.83	0.31
Recall	98.93	0.35	0.123	98.52	99.46	0.94	0.35
F-score	98.52	0.43	0.184	98.05	99.21	1.16	0.44
Dice Score	98.86	0.41	0.167	98.41	99.52	1.11	0.41

Table 12. Inter-dataset performance fluctuation

Metric	3Dircadb	Dataset 2	Dataset 3	Dataset 4	Dataset 5	Max. Fluctuation (%)
Accuracy	99.82	99.35	99.18	99.51	99.43	0.64
Precision	98.44	97.92	97.61	98.12	98.01	0.83
Recall	99.46	98.87	98.52	99.03	98.76	0.94
F-score	99.21	98.39	98.05	98.57	98.38	1.16
Dice Score	99.52	98.76	98.41	98.89	98.72	1.11

Table 13. Failure-case analysis of the proposed IQCSNN

Failure Case	Image Characteristics	Observed Segmentation Problem	Possible Cause	Expected Impact
Case 1	Extremely low-contrast tumor	Partial tumor region missed	Tumor intensity is very similar to surrounding liver parenchyma	Reduced Recall and Dice
Case 2	Very small lesion	Tiny lesion is partially or completely missed	Limited number of discriminative pixels and downsampling effects	Reduced Recall
Case 3	Highly heterogeneous tumor texture	Internal tumor region is fragmented	Strong intensity variation within the tumor	Reduced Precision and Dice
Case 4	Irregular tumor boundary	Boundary is slightly over- or under-segmented	Ambiguous transition between tumor and healthy tissue	Reduced boundary accuracy
Case 5	Tumor adjacent to vessels	False-positive regions near tumor	Similar intensity/texture characteristics of vessels and tumor	Reduced Precision
Case 6	Multiple closely located lesions	Neighboring lesions may be merged	Small separation between lesions and similar appearance	Reduced instance separation
Case 7	Very large infiltrative lesion	Peripheral tumor region is partially missed	Weak or diffuse tumor boundary	Reduced Recall and Dice

pixels and may contain insufficient spatial and textural information for reliable classification. Furthermore, feature extraction and resolution reduction within the neural network can cause very small lesions to become less prominent in deeper feature representations. This may result in false negatives or incomplete segmentation of small tumor regions. This limitation is particularly important because clinically relevant lesions can sometimes occupy only a very small portion of a CT slice.

Another challenging condition is heterogeneous tumor texture. Liver tumors may contain necrotic regions, hemorrhagic components, calcifications, or nonuniform enhancement patterns. Consequently, the intensity distribution within a single tumor can vary considerably. IQCSNN may correctly identify the dominant tumor region while incorrectly excluding low-intensity internal portions or producing fragmented predictions. Such cases primarily affect the Dice Score and Recall.

Irregular and poorly defined tumor boundaries also represent a limitation. When the transition between tumor and normal liver tissue is gradual rather than sharply defined, the ground-truth boundary itself may be difficult to distinguish from surrounding tissue. IQCSNN can therefore produce a slightly expanded or contracted boundary. Although the predicted region may remain visually close to the ground truth, small boundary deviations can noticeably affect pixel-level overlap metrics.

Tumors located near blood vessels or other anatomically similar structures constitute another source of false-positive predictions. Vessels can exhibit intensity and textural patterns that resemble portions of enhancing tumors. In such situations, the model may incorrectly classify a nearby vessel or vessel-adjacent region as tumor tissue. This indicates that spatial context and anatomical discrimination remain important areas for further improvement.

Cases containing multiple closely spaced lesions can

also be challenging. When two or more lesions have similar intensity characteristics and are separated by only a small number of pixels, the model may produce a connected segmentation region instead of clearly separating individual lesions. Conversely, very small lesions within a multi-lesion region may be omitted. This limitation becomes more evident in cases involving multiple heterogeneous tumors with substantially different sizes.

Overall, these failure cases demonstrate that the high average performance of IQCSNN does not imply perfect segmentation under all imaging conditions in Table 14. The principal limitations are associated with information-poor regions rather than the general segmentation architecture itself. Extremely low contrast, very small lesion size, heterogeneous internal texture, ambiguous boundaries, and anatomical similarity between tumors and surrounding structures can reduce the discriminative information available to the network.

Future work will therefore focus on incorporating higher-resolution multi-scale feature representations, explicit boundary-aware learning, small-lesion enhancement mechanisms, and more diverse multi-center training data. Attention mechanisms specifically designed for tiny lesions and contrast-enhancement strategies may further improve the detection of low-contrast tumors. Evaluation on larger external datasets acquired using different scanners and imaging protocols will also be necessary to establish the clinical robustness and generalization capability of IQCSNN.

3.5.1. Real-time feasibility

The deployment in clinical use could be constrained by hardware, latency in processing, and the necessity for high-speed quantum processors or quantum simulators, although this method is more accurate and robust in controlled settings. However, with the advancement of quantum computing infrastructure and Inspired frameworks optimised for this purpose, the technique has a strong potential for applications in real-time medical decision-making. While highly precise, the proposed IQCSNN-based liver tumor segmentation framework possesses some limitations, such as requiring large annotated training datasets that are not always available in clinical environments, and generalising across different imaging modalities, tumor categories, and patient populations is difficult. Hardware constraints, simulation overhead, and limited scalability for practical medical environments are additional challenges to integrating quantum-classical processing.

There are a number of practical and computational difficulties when integrating quantum computing with classical neural networks for large-scale medical datasets. First, because contemporary quantum devices (NISQ era) suffer from noise, decoherence, and restricted qubit capacity, the lack of scalable quantum hardware limits real-world implementation. Second, large-scale training is challenging because data encoding (quantum embedding) is computationally costly and presents a bottleneck when handling high-resolution medical images. Third, gradient instability and the requirement for parameter synchronization between quantum circuits and classical layers raise the complexity of training Inspired models. Furthermore, compared to purely classical models, computational overhead and latency are much higher, particularly when replicating quantum circuits on conventional machines. Practically speaking, adoption in clinical settings is hampered by a lack of standardized frameworks, high implementation costs, and a dearth of quantum machine learning competence. Furthermore, Inspired quantum models currently struggle to deliver the high dependability and interpretability needed for medical applications, which presents regulatory and validation issues. Despite the theoretical benefits of quantum-classical models, these problems collectively make their large-scale application difficult.

Role of quantum-classical functions in enhancing pixel-level tumor classification: Because they allow for richer and more expressive feature representations, quantum-classical functions in the IQCSNN model are essential to enhancing pixel-level tumor classification. The quantum component models intricate relationships between pixel intensities and spatial properties that are challenging for solely classical networks to represent by utilizing concepts like superposition and high-dimensional state encoding. These functions improve the model's capacity to discriminate between tumor and non-tumor pixels, even in situations with minute intensity variations, when combined with traditional sequential layers. This leads to better border identification, decreased misclassification, and increased segmentation accuracy overall.

Efficiency in managing photos of heterogeneous liver tumors with low contrast: Because of its Inspired architecture and strong preprocessing pipeline, the suggested IQCSNN model performs exceptionally well when handling low-contrast and diverse liver tumor pictures. While the quantum-classical feature extraction increases sensitivity to minor intensity changes and intricate texture patterns, the preprocessing processes, such as normalization and noise reduction, improve image quality. Furthermore, the model can adjust to irregular tumor forms and a variety of tissue features since the sequential neural network component captures spatial dependencies and contextual information. The model regularly produces accurate segmentation even

Table 14. Quantitative failure-case analysis

Tumor Condition	No. of Cases	Accuracy (%)	Precision (%)	Recall (%)	F-score (%)	Dice (%)
Normal/clear contrast	30	99.94	99.31	99.71	99.51	99.68
Low contrast	15	99.31	97.84	96.92	97.37	97.12
Tiny tumors	12	98.96	97.53	94.86	96.17	95.74
Heterogeneous texture	18	99.12	97.62	96.81	97.21	96.93
Irregular boundaries	15	99.24	97.91	97.16	97.53	97.28
Multiple lesions	10	99.08	97.45	96.38	96.91	96.67

in difficult imaging settings, exhibiting good robustness and generalization capability, as evidenced by the high Dice score and recall values.

3.5.2. Practical Implications and limitations

The proposed IQCSNN model has considerable implications for medical image analysis because it demonstrates how techniques from deep learning can be evolved and incorporated with quantum computing to solve complex problems in liver tumor segmentation. The technique can support the radiology community in early diagnosis and therapy planning, providing greater precision and reliability, thus improving patient outcomes and aiding precision medicine for cancer. The proposed IQCSNN will increase computational complexity due to Inspired quantum-classical processing and may require advanced hardware or simulation support. A limiting factor in the performance of the IQCSNN is that it requires well-annotated datasets, which are very difficult to obtain in a clinical setting. There are challenges in generalizing findings across different imaging devices and patient populations, which need further validation. The proposed IQCSNN has several advantages, including its potential to achieve generality by delivering consistent performance across various benchmark databases. Nonetheless, the model's design, which focuses on incorporating spatial and sequential information, contributes to robustness and resistance to changes in tumor dimensions and contrast. Variability is also likely to include imaging protocols, manufacturers, and population diversity, but the proposed model needs to be validated to assess its potential for achieving generality.

It is crucial to make clear that neither physical quantum hardware implementation nor the use of explicit quantum computing platforms like Qiskit or PennyLane are part of the suggested IQCSNN framework. Rather, the model uses a Inspired approach inspired by quantum computing, including some quantum computation concepts, like complex correlation modeling and high-dimensional feature representation, within a classical neural network design. While retaining computational viability on classical systems, these quantum-inspired techniques are intended to increase segmentation performance and feature extraction. Therefore, rather than referring to a true qubit-based implementation, the phrase "Inspired quantum-classical" in this study refers to the conceptual integration of quantum-inspired processes with classical sequential learning. This explanation guarantees openness and prevents the suggested methodology from being misunderstood.

Quantum circuit integration with classical neural networks results in higher training times and computational resources, thus making the proposed IQCSNN framework more complex than conventional models. The better capability of acquiring complex attributes of tumors to enhance the segmentation process makes the extra complexity worth the effort. This model can scale up for use in extensive data sets in powerful computers, although its scalability may be limited due to quantum simulation costs through methods such as mini-batch learning, patch learning, and mixed optimization. All three aspects of the proposed IQCSNN's computation time, inference delay, and hardware efficiency have been considered appropriately. More computing power will be required for training owing to the use of Inspired quantum and classical processors, while inference latency remains relatively short and can be further minimized with GPU computing and proper quantum circuit simulation. Thus, the model could prove useful in real-time clinical assistance, although not in a strict sense. Moreover, an analysis of errors has been conducted, which reveals that there could be a decline in the effectiveness of the system when encountering challenging samples, such as those containing small or poorly contrasted tumors. However, even under these circumstances, Inspired feature extraction exhibits increased robustness compared to traditional approaches.

4. Conclusion

This work filled a key research gap in liver tumor segmentation, where low-contrast pictures, diverse tumor shapes, and restricted feature representation capabilities are challenges for current traditional deep learning models.

In order to get over these restrictions, a brand-new Inspired Quantum-Classical Sequential Neural Network (IQCSNN) was put forth with the goal of improving seg-

mentation accuracy by combining sequential deep learning with quantum-inspired feature extraction.

By combining reliable preprocessing, effective feature extraction, and pixel-level classification, the suggested framework effectively achieved the goal by facilitating better tumor and non-tumor region identification.

The model's capacity to capture intricate spatial and intensity variations—which are usually overlooked by traditional methods—was greatly improved by the use of quantum-classical functions.

The effectiveness of the IQCSNN model is validated by experimental results, which show that it achieves superior performance across all evaluation metrics, including accuracy (99.82%), recall (99.46%), precision (98.44%), F-score (99.21%), and Dice score (99.52%), along with a very low error rate (0.0018).

Additionally, the model demonstrated remarkable efficacy in managing diverse and low-contrast tumor images, guaranteeing improved tumor boundary delineation and decreased misclassification.

Notwithstanding these advancements, the paper highlights significant obstacles such high computational complexity, restricted access to quantum technology, and scalability problems for extensive medical datasets.

Furthermore, the need for better generalization across a range of clinical circumstances is highlighted by variations in imaging modalities and tumor features. Future research will concentrate on optimizing quantum-classical integration for increased efficiency and scalability, integrating multimodal imaging methods (such as PET-CT and ultrasound), and expanding the IQCSNN framework to bigger and more varied datasets.

References

[1] P. Bilic, P. Christ, H. B. Li, E. Vorontsov, A. Ben-Cohen, G. Kaissis, and B. Menze, (2023) *"The Liver Tumor Segmentation Benchmark (LiTS)"* **Medical Image Analysis *84***: 102680. DOI: 10.1016/j.media.2022.102680.

[2] J. Wang, Y. Peng, S. Jing, L. Han, T. Li, and J. Luo, (2023) *"A Deep-Learning Approach for Segmentation of Liver Tumors in Magnetic Resonance Imaging Using UNet++"* **BMC Cancer *23***(1): 1060. DOI: 10.1186/s12885-023-11432-x.

[3] G. Chen, Z. Li, J. Wang, J. Wang, S. Du, J. Zhou, and Y. Zhou, (2023) *"An Improved 3D KiU-Net for Segmentation of Liver Tumor"* **Computers in Biology and Medicine *160***: 107006. DOI: 10.1016/j.compbiomed.2023.107006.

[4] S. Di, Y. Q. Zhao, M. Liao, F. Zhang, and X. Li, (2022) *"TD-Net: A Inspired End-to-End Network for Automatic Liver Tumor Segmentation from CT Images"* **IEEE Journal of Biomedical and Health Informatics *27***(3): 1163–1172. DOI: 10.1109/JBHI.2022.3181974.

[5] J. Amin, M. A. Anjum, M. Sharif, S. Kadry, and R. G. Crespo, (2023) *"Visual Geometry Group Based on U-Shaped Model for Liver/Liver Tumor Segmentation"* **IEEE Latin America Transactions *21***(4): 557–564. DOI: 10.1109/TLA.2023.10128927.

[6] Y. Chen, C. Zheng, W. Zhang, H. Lin, W. Chen, G. Zhang, and F. Wu, (2023) *"MS-FANet: Multi-Scale Feature Attention Network for Liver Tumor Segmentation"* **Computers in Biology and Medicine *163***: 107208. DOI: 10.1016/j.compbiomed.2023.107208.

[7] C. Zhang, J. Lu, Q. Hua, C. Li, and P. Wang, (2022) *"SAA-Net: U-Shaped Network with Scale-Axis-Attention for Liver Tumor Segmentation"* **Biomedical Signal Processing and Control *73***: 103460. DOI: 10.1016/j.bspc.2021.103460.

[8] J. Li, K. Liu, Y. Hu, H. Zhang, A. A. Heidari, H. Chen, and H. Elmannai, (2023) *"Eres-UNet++: Liver CT Image Segmentation Based on High-Efficiency Channel Attention and Res-UNet++"* **Computers in Biology and Medicine *158***: 106501. DOI: 10.1016/j.compbiomed.2022.106501.

[9] X. Wang, S. Wang, Z. Zhang, X. Yin, T. Wang, and N. Li, (2023) *"CPAD-Net: Contextual Parallel Attention and Dilated Network for Liver Tumor Segmentation"* **Biomedical Signal Processing and Control *79***: 104258. DOI: 10.1016/j.bspc.2022.104258.

[10] S. Di, Y. Zhao, M. Liao, Z. Yang, and Y. Zeng, (2022) *"Automatic Liver Tumor Segmentation from CT Images Using Hierarchical Iterative Superpixels and Local Statistical Features"* **Expert Systems with Applications *203***: 117347. DOI: 10.1016/j.eswa.2022.117347.

[11] F. Lyu, M. Ye, A. J. Ma, T. C. F. Yip, G. L. H. Wong, and P. C. Yuen, (2022) *"Learning from Synthetic CT Images via Test-Time Training for Liver Tumor Segmentation"* **IEEE Transactions on Medical Imaging *41***(9): 2510–2520. DOI: 10.1109/TMI.2022.3166230.

[12] X. Wang, X. Zhang, G. Wang, Y. Zhang, X. Shi, H. Dai, and X. Meng, (2022) *"TransFusionNet: Semantic and Spatial Features Fusion Framework for Liver Tumor and Vessel Segmentation under JetsonTX2"* **IEEE Journal of Biomedical and Health Informatics *27***(3): 1173–1184. DOI: 10.1109/JBHI.2022.3207233.

[13] M. Rela, N. R. Suryakari, and R. R. Patil, (2023) *"A Diagnosis System by U-Net and Deep Neural Network Enabled with Optimal Feature Selection for Liver Tumor Detection Using CT Images"* **Multimedia Tools and Applications** ***82***(3): 3185–3227. DOI: 10.1007/s11042-022-13381-2.

[14] D. T. Kushnure, S. Tyagi, and S. N. Talbar, (2023) *"LiM-Net: Lightweight Multi-Level Multi-Scale Network with Deep Residual Learning for Automatic Liver Segmentation in CT Images"* **Biomedical Signal Processing and Control** ***80***: 104305. DOI: 10.1016/j.bspc.2022.104305.

[15] F. Zhan, W. Wang, Q. Chen, Y. Guo, L. He, and L. Wang, (2023) *"Three-Direction Fusion for Accurate Volumetric Liver and Tumor Segmentation"* **IEEE Journal of Biomedical and Health Informatics** ***28***(4): 2175–2186. DOI: 10.1109/JBHI.2023.3344392.

[16] K. N. Wang, S. X. Li, Z. Bu, F. X. Zhao, G. Q. Zhou, S. J. Zhou, and Y. Chen, (2024) *"SBCNet: Scale and Boundary Context Attention Dual-Branch Network for Liver Tumor Segmentation"* **IEEE Journal of Biomedical and Health Informatics** ***28***(5): 2854–2865. DOI: 10.1109/JBHI.2024.3370864.

[17] H. Rahman, N. B. Aoun, T. F. N. Bukht, S. Ahmad, R. Tadeusiewicz, P. Pławiak, and M. Hammad, (2025) *"Automatic Liver Tumor Segmentation of CT and MRI Volumes Using Ensemble ResUNet-InceptionV4 Model"* **Information Sciences** ***704***: 121966. DOI: 10.1016/j.ins.2025.121966.

[18] Y. Ni, G. Chen, Z. Feng, H. Cui, D. Metaxas, S. Zhang, and W. Zhu, (2024) *"DA-Tran: Multiphase Liver Tumor Segmentation with a Domain-Adaptive Transformer Network"* **Pattern Recognition** ***149***: 110233. DOI: 10.1016/j.patcog.2023.110233.

[19] D. Cheng, Z. Zhou, and J. Zhang, (2024) *"EG-UNETR: An Edge-Guided Liver Tumor Segmentation Network Based on Cross-Level Interactive Transformer"* **Biomedical Signal Processing and Control** ***97***: 106739. DOI: 10.1016/j.bspc.2024.106739.

[20] H. Liu, J. Yang, C. Jiang, S. He, Y. Fu, S. Zhang, and W. Ji, (2024) *"S2DA-Net: Spatial and Spectral-Learning Double-Branch Aggregation Network for Liver Tumor Segmentation in CT Images"* **Computers in Biology and Medicine** ***174***: 108400. DOI: 10.1016/j.compbiomed.2024.108400.

[21] L. Zhang, W. Zhang, and Z. Xu, (2025) *"Automatic Liver Tumor Segmentation Based on Improved YOLO-v5 and B-Spline Level Set"* **Cluster Computing** ***28***(3): 214. DOI: 10.1007/s10586-024-04918-1.

[22] R. Kılıç, A. Yalçın, F. Alper, E. A. Oral, and I. Y. Ozbek, (2025) *"Two-Stage Automatic Liver Classification System Based on Deep Learning Approach Using CT Images"* **Journal of Imaging Informatics in Medicine**: 1–23. DOI: 10.1007/s10278-025-01480-z.

[23] K. Trivedi, (2025) *"Optimization Approaches Using Machine Learning Techniques to Preidentification of Liver Cancer"* **NanoMind: Exploring Synergies in Nanotechnology and Machine Learning**: 151–195. DOI: 10.1007/978-3-031-77296-2_8.

[24] G. Aksholak, A. Bedelbayev, R. Magazov, and K. Kaplan, (2026) *"Transformer Tokenization Strategies for Network Intrusion Detection: Addressing Class Imbalance Through Architecture Optimization"* **Computers** ***15***(2): 75. DOI: 10.3390/computers15020075.

[25] R. Jin, H. Y. Tang, Q. Yang, and W. Chen, (2025) *"LA-ResUNet: Attention-Based Network for Longitudinal Liver Tumor Segmentation from CT Images"* **Computerized Medical Imaging and Graphics** ***123***: 102536. DOI: 10.1016/j.compmedimag.2025.102536.

[26] A. B. Slama, H. Sahli, Y. Amri, and S. Labidi, (2025) *"V-NET-VGG16: Inspired Deep Learning Architecture for Optimal Segmentation and Classification of Multi-Differentiated Liver Tumors"* **Intelligence-Based Medicine** ***11***: 100210. DOI: 10.1016/j.ibmed.2025.100210.

[27] J. Zhao and S. Li, (2025) *"Uncertainty-Guided and Cross-Modality Attention Network for Liver Tumor Segmentation and Quantification via Integrating Dynamic MRI"* **Knowledge-Based Systems** ***310***: 113021. DOI: 10.1016/j.knosys.2025.113021.

[28] P. Sivanagaraju, S. V. Ramana, and P. P. Reddy, (2025) *"An Advanced Transformer Framework for Liver Tumor Segmentation Using MRI Images"* **Biomedical Signal Processing and Control** ***107***: 107808. DOI: 10.1016/j.bspc.2025.107808.

[29] G. N. Yashaswini, R. V. Manjunath, B. Shubha, P. Prabha, N. Aishwarya, and H. M. Manu, (2025) *"Deep Learning Technique for Automatic Liver and Liver Tumor Segmentation in CT Images"* **Journal of Liver Transplantation** ***17***: 100251. DOI: 10.1016/j.liver.2024.100251.

[30] L. W. Tsai, A. Agrawal, P. Dash, S. Panda, Y. W. Huang, S. Saxena, and C. M. Shih, (2025) *"RFiLM U-Net: Radiomic Feature-Integrated Linear Modulation Network for Precise Liver Tumor Segmentation"* **Journal of Medical and Biological Engineering *45***(2): 177–186. DOI: 10.1007/s40846-025-00938-3.

[31] J. K. Appati, N. A. Azuponga, L. M. Boante, and J. A. Mensah, (2024) *"A Multiattention ResUNet and Modified U-Net Architecture for Liver Tumor Segmentation"* **Applied Computational Intelligence and Soft Computing *2024***(1): 8365349. DOI: 10.1155/2024/8365349.

[32] M. Reyad, A. M. Sarhan, and M. Arafa, (2024) *"Architecture Optimization for Inspired Deep Residual Networks in Liver Tumor Segmentation Using a GA"* **International Journal of Computational Intelligence Systems *17***(1): 209. DOI: 10.1007/s44196-024-00542-4.

[33] Y. Challagundla, T. S. C. Tunuguntla, S. G. Tunuguntla, and N. Devarakonda, (2025) *"Convolutional Neural Network-Based Classifiers for Liver Tumor Detection Using Computed Tomography Scans"* **Innovations in Systems and Software Engineering *21***(2): 533–539. DOI: 10.1007/s11334-023-00547-w.

[34] C. Bai, W. Shi, M. Zhang, and H. Zhao, (2026) *"CrackDualMamba: A Lightweight Dual-Stream Mamba with Novel Focal Dice Balanced Loss for Vehicle-Based Road Crack Segmentation"* **Advanced Engineering Informatics *71***: 104427. DOI: 10.1016/j.aei.2026.104427.

[35] J. Zhang, C. Bai, W. Pan, and J. Guo, (2026) *"Virtual-Force Based Visual Servo for Multiple Peg-in-Hole Assembly With Tightly Coupled Multi-Manipulator"* **IEEE Robotics and Automation Letters *11***(3): 2586–2593. DOI: 10.1109/LRA.2026.3653374.

[36] A. B. Sawad and M. Binsawad, (2026) *"Radiomics-Driven Inspired Deep Learning for MRI-Based Prediction of Glioma Grade and 1p/19q Codeletion"* **Tomography *12***(2): 25. DOI: 10.3390/tomography12020025.

[37] B. A. Alqaralleh, M. Z. Alksasbeh, A. Kulakli, and A. I. Zreikat, (2026) *"An Intelligent Healthcare Framework for Hepatocellular Carcinoma Diagnosis Based on Aggregated Learners from Biomedical Data Utilizing Explainable Artificial Intelligence"* **Scientific Reports *16***: 9357. DOI: 10.1038/s41598-026-39871-z.

[38] E. Lanza, A. Ammirabile, A. Vanzulli, C. Lisi, A. S. Perera, A. M. A. Lucia, and A. Laghi, (2026) *"3D Region-Growing nnU-Net Improves Pulmonary Embolism Detection on CTPA: A Dual-Cohort Validation Study"* **European Radiology Experimental *10***(1): 23. DOI: 10.1186/s41747-026-00693-3.

[39] P. Sun, J. Yu, Q. Gu, L. Zhang, Y. Sun, Q. Wang, and J. Zhu, (2026) *"Clinically Oriented Automatic 2D Liver Tumor Segmentation: LCMambaNet with a State-Space Model and Liver Cancer-Specific Attention"* **Frontiers in Oncology *16***: 1676424. DOI: 10.3389/fonc.2026.1676424.

[40] A. I. Abian, R. K. Debnath, M. A. Rahman, M. A. K. Raiaan, M. R. Islam, A. Karim, and S. Azam, (2026) *"HANS-Net: Hyperbolic Convolution and Adaptive Temporal Attention for Accurate and Generalizable Liver and Tumor Segmentation in CT Imaging"* **IEEE Transactions on Radiation and Plasma Medical Sciences**: DOI: 10.1109/TRPMS.2026.3654628.